Peposertib suppresses generation of *FLT3*-internal tandem duplication formed by contralateral double nicks

Shota Yoshida[1], Masahiro Onozawa[1], Shota Yokoyama[1], Toshihiro Matsukawa[1], Hideki Goto[1], Shinsuke Hirabayashi[2], Takeshi Kondo[3], Daigo Hashimoto[1], Yasuhito Onodera[4], Takanori Teshima[1]

[1] Department of Hematology, Hokkaido University Faculty of Medicine, Graduate school of Medicine, Sapporo, Japan
[2] Department of Pediatrics, Faculty of Medicine, Graduate School of Medicine, Hokkaido University, Sapporo, Japan
[3] Blood Disorders Center, Aiiku Hospital, Sapporo, Japan
[4] Global Center for Biomedical Science and Engineering (GCB), Faculty of Medicine, Hokkaido University, Sapporo, Japan

Abstract word count: 214words

Highlights: 3 sentences

Text word count: 3,685 words

The number of figures and tables: 5 figures

Supplementary information: 1

Supplementary dataset: 1

Reference: 46 references

Corresponding author:
Masahiro Onozawa
Department of Hematology
Hokkaido University Faculty of Medicine, Graduate school of Medicine
Kita 15, Nishi 7, Kita-Ku, Sapporo, JAPAN 0608638
Tel: +81-11-706-7214
onozawa@med.hokudai.ac.jp

Artificial *FLT3*-ITD generation

Where *FLT3*-ITD is expected to form endonuclease

Contralateral double nicks

FLT3 exon 14 5' 3' 3' 5'

Double-strand break (DSB) with protruding ends

Repair in leading strand + DNA-end resection

Replication forks passing each other

Near blunt ends initiate NHEJ

±NNN (filler)

DSB repair by non-homologous end joint (NHEJ)

FLT3-ITD

Peposertib

FLT3-ITDs found in AML

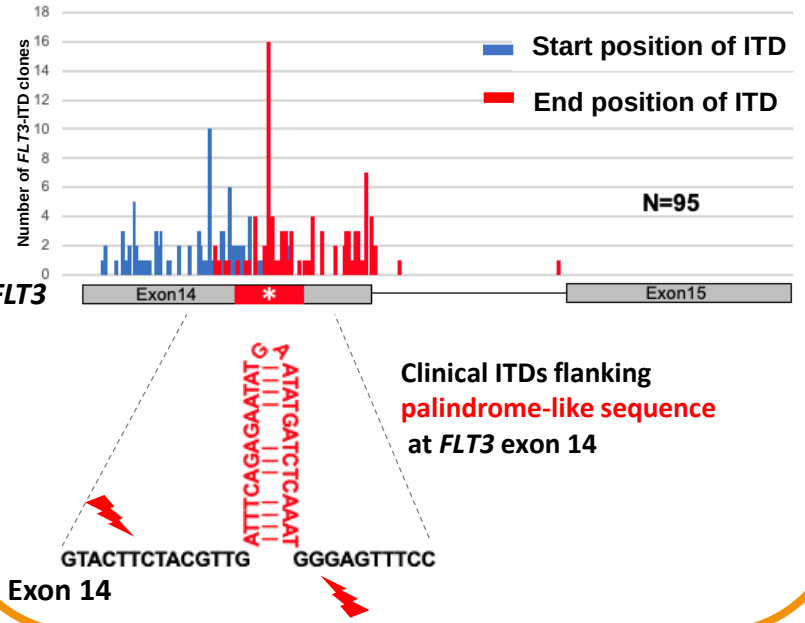

K562

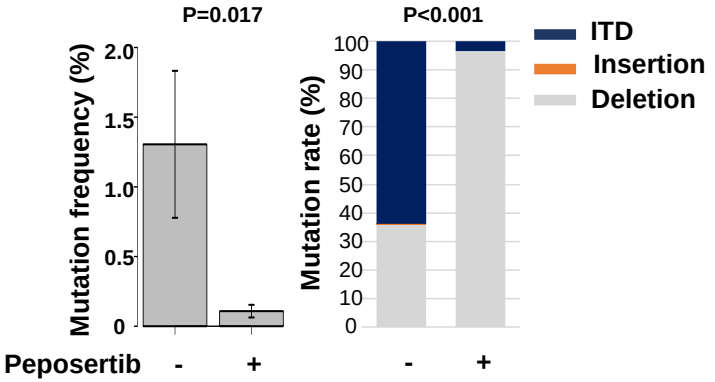

Highlights:

- Contralateral double nicks were effectively repaired as *FLT3*-ITD.
- Peposertib remarkably reduced mutation frequency and ITD formation.
- Non-homologous end joining (NHEJ) is indispensable to the generation of *FLT3*-ITDs.

Abstract

FLT3-internal tandem duplication (ITD) is the most frequent gene mutation in acute myeloid leukemia. The consequences of *FLT3*-ITD have been analyzed in detail; however, the molecular mechanisms underlying *FLT3*-ITD generation have remained to be elucidated. We analyzed *FLT3*-ITDs in clinical samples using deep sequencing and identified not only oligoclonal ITDs but also rare deletion clones clustered at the palindrome-like sequence at *FLT3* exon 14. We hypothesized that *FLT3* exon 14 is genetically unstable due to the palindrome-like sequence at the region and that genomic damage at the site initiates *FLT3*-ITD formation. We used CRISPR/Cas9 to induce DNA damage for creating artificial *FLT3*-ITDs in human and mouse cell lines. We found that double nicks on the adjacent contralateral strand most efficiently generate ITDs. The artificial ITDs resembled clinical ITDs in the length distribution and characteristics at the joint. We further compared the inhibitory effects of olaparib and peposertib, specific inhibitors of single-strand break (SSB) and DSB repair, respectively. Peposertib remarkably reduced ITD formation, but olaparib did not affect the mutation pattern. The findings indicated that non-homologous end joining has a crucial role in the generation of ITDs. Our data shed light to the new role of peposertib, which potentially suppress generation of de-novo *FLT3*-ITDs caused by mis-repair event of the DNA damages in clinical course.

Key word: *FLT3*-ITD, acute myeloid leukemia, Double-strand break, CRISPR/Cas9, non-homologous end joining, Peposertib

Introduction

The fms-like tyrosine kinase 3-internal tandem duplication (*FLT3*-ITD) is the most common driver mutation in acute myeloid leukemia (AML) [1, 2]. Various numbers of nucleotide elongation occurs in multiples of three (3N), preserving the reading frame, which results in ligand-independent transduction of the signal and cell proliferation via STAT5 phosphorylation in clinical samples [3]. Although inhibitors of *FLT3*-ITD have been developed, their effects are transient and treatment with the agents has not provided a cure. Further improvement in the prognosis is desired because AML with *FLT3*-ITD has a high relapse rate [4-6].

FLT3-ITD is an unstable mutation that can appear at relapse in patient who was initially *FLT3*-ITD-negative or disappear at relapse in a patient who was initially *FLT3*-ITD-positive [7-11]. The consequences of *FLT3*-ITD have been analyzed in detail; however, the molecular mechanisms underlying *FLT3*-ITD generation remain to be elucidated [12-14]. We notified that palindromic sequences are identified at recurrent tandem duplication sites in *FLT3* exon 14, *NPM1* exon 12, and *UBTF* exon 12 (Fig. S1). Genomic instability is a hallmark of AML with *FLT3*-ITD [4, 15, 16]. We identified rare deletion event at *FLT3*-ITD cluster region by deep sequencing and hypothesized that mis-repair event of genomic damage at the site cause *FLT3*-ITD. To elucidate the precise mechanisms underlying the generation of *FLT3*-ITD, we examined the different modes of DNA damage induced by clustered regularly interspaced short palindromic repeats (CRISPR)/Cas9 system using various cell lines.

Materials and Methods

Patients

Twenty cases of AML with *FLT3*-ITD that were registered in Hokkaido Leukemia Net (HLN) were randomly selected and *FLT3*-ITD was analyzed by next-generation sequencing (NGS). The HLN is a multicentric prospective observational cohort study collecting acute leukemia samples from affiliated hospitals covering Hokkaido (UMIN000048611) [17]. This study was conducted in accordance with the Helsinki Declaration and was approved by the institutional review board of Hokkaido University Hospital (#015-0344). Written consent was obtained from all patients.

Cell cultures and reagents

HEK293T cells (human embryonic kidney cells) and K562 cells (chronic myeloid leukemia cells) were purchased from Japanese Collection of Research Bioresources (JCRB, Osaka, Japan). Ba/F3 cells (cell line from mouse B cells) were purchased from ATCC (Manassas, VA). HEK293T cells were cultured in Dulbecco's modified Eagle's medium (DMEM) with 10% fetal calf serum (FCS) and 1% penicillin/streptomycin (PS). K562 cells were cultured in RPMI1640 medium with 10% FCS and 1% PS. Ba/F3 cells were cultured in RPMI1640 medium with 10% FCS, 1% PS, and 10 ng/ml of recombinant mouse IL-3 (BioLegend, San Diego). Olaparib (AZD2281), a poly (ADP-ribose) polymerases (PARP) 1/2

inhibitor, was purchased from Chemexpress (Shanghai, China) and peposertib (M3814), a DNA activated protein kinase catalytic subunit (DNA-PKcs) inhibitor, was purchased from Selleckchemicals (Houston, TX).

Artificial human *FLT3*-ITD and mouse *Flt3*-ITD generation by the CRISPR/Cas9 system

We generated cell lines with Doxycycline (Dox)-inducible Cas9 nuclease (Document S1). Cas9-expressing cells were transfected with 500 ng of gRNA (Invitrogen) targeting the flanking region of the palindrome-like sequence of human *FLT3* exon 14 (h*FLT3* exon 14S: 5'-AATATGAATATGATCTCAAA-3', h*FLT3* exon 14AS: 5'-GTAGAAGTACTCATTATCTG-3') or mouse *Flt3* exon 14 (m*Flt3* exon 14S: 5'-ACTATGAATATGACCTTAAG-3', m*Flt3* exon 14AS: 5'-TATCCAGGGGGCCAGTCACC-3') .

***FLT3*-ITD assay and definition of mutation clones**

Genomic DNA (> 100 ng) was purified from each cell line and PCR-amplified with a human *FLT3* primer set (Forward: 5'-GCAATTTAGGTATGAAAGCCAGC-3' and Reverse: 5'-CTTTCAGCATTTTGACGGCAACC-3') or a mouse *Flt3* primer set (Forward: 5'-CTCTGCAGCGCTGCTGACC-3' and Reverse: 5'-CTCTGAGGGACTTTGCTGAG-3'). PCR was performed in a 20 μL reaction containing 12.5 U of PrimeSTAR GXL DNA Polymerase (Takara Bio inc., Shiga, Japan), and 100 ng of template DNA. The thermal cycling conditions were: initial denaturation at 98°C for 3 min; followed by 34 cycles of 98°C for 10 sec, 60°C for 15 sec, and 68°C for 30 sec; and a final extension at 68°C for 4 min.

PCR products were deep-sequenced by NGS at Research Institute for Microbial Disease, Osaka University (Osaka, Japan) using Miseq (Illumina, San Diego, CA). Reference sequences of the PCR product were 329 bp for human *FLT3* and 400 bp for mouse *Flt3*. Shortening and elongation events 3 bp or more were defined as mutation events, and the sequences were analyzed by a BLAT search (https://genome.ucsc.edu/cgi-bin/hgBlat). Clones with 2 or more reads were analyzed. In the analysis, we defined "mutation frequency" as the ratio of total mutant clone reads to the total number of reads and we defined "mutation rate" as the ratio of clone number of each mutant category in the total mutant clones.

Western blotting

Protein expression were analyzed using following antibodies: anti-HA-tag monoclonal antibody (MBL, Nagoya, Aichi, Japan), anti-β-actin antibody mouse monoclonal (Sigma-Aldrich, St. Louis, MO), anti-phospho-H2AX (Ser139) antibody (Sigma-Aldrich), DNA-PKcs polyclonal antibody (Proteintech, IL, USA), anti-DNA PKcs (phospho 2056) antibody (Abcam, Cambridge, UK).

Statistical analysis

A two-tailed unpaired t-test was used for comparison of mutation frequencies and mutation rates in cell proliferation assays, comparison of the efficiency of *FLT3*-ITD generation by repair pathway inhibition and comparison of the expression of NHEJ associated factors in clinical samples. The Mann–Whitney U test was used to compare continuous values in comparison of VAFs of clinical *FLT3*-ITDs and deletions. Statistical significance was defined as a P value < 0.05. Statistical analyses were performed with EZR ver 1.52 [18].

Results

Deep sequencing of clinical *FLT3*-ITD revealed DNA damage repair signature

We analyzed *FLT3*-ITD in clinical samples using NGS. In 20 cases of AML with *FLT3*-ITD, 95 ITD clones, 1 insertion (ins) clone, and 8 deletion (del) clones were detected (Table S1). Oligoclonal clones with ITDs could be found in a single case. A median of 3.5 ITD clones per case were detected. The start and end of the duplicated region were clustered at *FLT3* exon 14 (Fig. 1A). In the middle of the ITD cluster, there was a palindrome-like sequence stretching for 30 bp (Fig. 1B). The uncomplete palindrome showed 11 paired matches within the 30 bp. Deep sequencing also revealed rare clones with a deletion in the region (Fig. 1C). The VAF of the ITDs varied from 0.0014% to 45.7%, the VAF of deletions was always less than 0.01% (Fig. 1D). The median length of ITDs was 51 bp (6-192 bp) (Fig. 1E). The ITDs were all in-frame mutations consisting of elongations of multiples of 3 (3N) bp except for one non-3N ITD with VAF less than 0.01% (Fig. 1F). Co-occurrence of ITD and del mutation in the same region suggested that DNA damage at the site initiates the mutation process. A hairpin structure induced by the palindrome-like sequence is considered to be genetically unstable and prone to be mutated [19]. We further verified the sequences of *FLT3*-ITDs and categorized the ITD events into the following three groups: I) ITD clones without an additional nucleotide (filler) or homologous sequence at the joint of ITD (n=51, 53.7%), II) ITD clones with a filler at the joint of ITD (n=40, 42.1%) and III) ITD clones with microhomology at the ITD joint (n=4, 4.2%) (Fig. 1G, S2). In this study, it was defined as ITD with microhomology when the sequence at the 5' end of the ITD and the sequence immediately following the end of the ITD had a homology of 2 bp or more.

Artificial *FLT3*-ITD generation by different modes of DNA damage induced by the CRISPR/Cas9 system

We hypothesized that ITD is caused by mis-repair event of DNA damage. To elucidate the hypothesis, we established HEK293T, K562, TF-1, and Ba/F3 cell lines with Dox-inducible DSBs by CRISPR Cas9 and SSB by CRISPR Cas9-nikase (D10A or H840A) using a piggyBac transposon vector (Fig. 2A, S3). We compared different modes of DNA damage including single DSB, double DSBs, single SSB and double SSBs (Fig. 2B). A pair of gRNAs were designed to target the sites flanking the palindrome-like sequence within human *FLT3*

exon 14 (Fig. 2C). Single gRNA (h*FLT3* exon 14S or h*FLT3* exon 14AS) or double gRNAs (h*FLT3* exon 14S and h*FLT3* exon 14AS) were transfected into the Tet-on-Cas9-DSB or nickase cell lines (Fig. 2B, C). Examples of artificial *FLT3*-ITD sequences obtained in K562 cell line were shown (Fig. 2D).

Contralateral double nicks more efficiently generated *FLT3*-ITD than did DSBs or single nick

We compared mutation events of the artificial genome damage using HEK293T cells and K562 cells in which the expression of Cas9-DSB and Cas9-D10A was induced by Dox. DSB were mostly repaired by del and a few ins (Fig. 3A). Mutation events of SSB were much less than those of DSB, indicated that SSB could be efficiently repaired without a scar (Fig. 3A). On the other hand, contralateral double nicks generated more ITD clones than did DSB (Fig. 3A). Using the same gRNA pair, we also verified 3' overhang-double nicks induced by Cas9-H840A (Fig. S4A). Although mutation frequency of 3' overhang were lower than that of 5' overhang, the ITD rate was significantly higher in HEK293T cells and no significant difference was observed in K562 cells (Fig. S4B). These results suggested that contralateral double nicks efficiency generated ITDs. Because mutation frequency of Cas9-D10A was higher than Cas9-H840A, we used Cas9-D10A for further analysis.

The region of the duplicated sequence was always located within two nicks (Fig. 3B, Supplementary dataset). The distribution of lengths of the ITDs were varied and similar among the cell lines and clinical samples (Fig. 3C). Elongation lengths were equally distributed among 3N, 3N+1, and 3N+2 bp (Fig. 3D). We verified the sequences of 381 *FLT3*-ITD clones generated in HEK293T cells and 439 *FLT3*-ITD clones generated in K562 cells by contralateral double nicks. Two hundred eighty-six (75.1%) and 305 (69.5%) *FLT3*-ITD clones had neither fillers nor homologous sequences at the ITD ends in HEK293T cells and K562 cells. Fillers were detected in 49 (12.9%) and 87 (19.8%) of the ITD clones, respectively. The other 46 (12%) ITD clones and 47 (10.7%) ITD clones had microhomology at the ITD joint (Fig. 3E). We also tried human AML cell line, TF-1 cells to create artificial *FLT3*-ITD (Fig. S5A-E, Supplementary dataset). Although the mutation frequency was significantly lower, the characteristics of the *FLT3*-ITD were similar to those of HEK293T and K562 cells (Fig. S5A-E).

Furthermore, spontaneous *Flt3*-ITD was reported in murine AML models including radiation-induced AML and CALM-AF10 transgenic mice [20, 21]. Murine *Flt3* also has a palindrome-like sequence showing 10 paired matches within 30 bp at the *Flt3* exon 14 (Fig. S6). We performed an experiment using Cas9 inducible Ba/F3 cells to verify the characteristics of artificial *Flt3*-ITD (Fig. S3, S7). Similar to human cells, the contralateral double nicks most effectively created ITDs (Fig. S7A). Duplicated sequences were clustered in the middle of the cleavage sites (Fig. S7B, Supplementary dataset). The distributions of the lengths of ITDs and classification of the joint were similar to those of human HEK293T and K562 cells (Fig. S7C-E).

We also conducted a long-term culture of the *FLT3*-ITD induced K562 cells to whether the *FLT3*-ITD containing clones expand in frequency. We serially analyzed the population of clones with *FLT3*-ITD, however, the frequency of the clones with *FLT3*-ITD was not increased (Fig. S8). Our model cell lines did not express *FLT3* protein, therefore, not adequate for functional assay of biological consequences of *FLT3*-ITD.

FLT3-ITD generation was suppressed by inhibition of DSB repair but not by inhibition of SSB repair

Olaparib is an inhibitor of PARP1/2, which contributes repairing SSBs by base excision repair (BER) [22]. We investigated whether administration of olaparib affects *FLT3*-ITD generation efficiency at a concentration that does not have a negative effect on cell proliferation (Fig. S9). Expression of γ-H2AX was increased by transfection of gRNAs and administration of olaparib in each cell line (Fig. 4A). Neither mutation frequency nor frequency of ITD events was changed by olaparib treatment (Fig. 4A). Inhibition of the SSB repair pathway by olaparib did not suppress *FLT3*-ITD generation. Increased expression of γ-H2AX suggested that the DSB repair pathway was activated when contralateral double nicks were induced.

Peposertib inhibits the activity of DNA-PK, thereby interfering with the NHEJ process and preventing repair of DSBs [23, 24]. We investigated whether administration of peposertib reduces *FLT3*-ITD generation efficiency at a concentration that does not have a negative effect on cell proliferation (Fig. S9). HEK293T cells and K562 cells treated with or without peposertib were harvested at 0, 4, 8, 12, 48 hours after transfection of gRNAs. It was confirmed that the expression of DNA-PKcs autophosphorylation that was decreased by peposertib treatment (Fig. 4B). Mutation frequency was significantly reduced by peposertib administration. Moreover, the rate of *FLT3*-ITD events was significantly reduced by peposertib treatment (Fig. 4B). We also generated cell lines with Dox-inducible wild-type *FLT3* and *FLT3*-ITD to analyze whether peposertib differentially impact the growth/survival of *FLT3*-ITD mutant clones compared to wild-type clones (Fig. S10). Peposertib treatment used in current study did not affect the cell growth of cells with wildtype *FLT3* and *FLT3*-ITD (Fig. S10). This result showed decreased frequency of ITDs reflected decreased creation of ITDs, not due to selective killing of cells with FLT3-ITD. To exclude the possibility of non-specific suppression of peposertib, we confirmed the finding was reproducible using K562 cells with DNA-PKcs knock out (Fig. 4C, Document S2). These results showed that the NHEJ process plays an important role in the generation of *FLT3*-ITDs.

DNA-PKcs, Ku80 expressed higher in cases with *FLT3*-ITD or *NPM1* mutated

FLT3-ITD is considered as relatively later event and preferentially arise from certain genetic backgrounds such as *NPM1* mutation, *NUP98::NSD1*, or *DEK::NUP214* [25-27]. In AML with *NPM1* mutation, *FLT3*-ITD is enriched (45.3%) and acquisition of an *FLT3*-ITD clone at relapse occurred in up to 40% of cases [27, 28]. We hypothesized that AML with

NPM1 mutation would have activated NHEJ pathway which confer the cell to yield de novo *FLT3*-ITD clones. Therefore, we compared the expression of NHEJ-related factors: DNA-PKcs, Ku80, Ku70 and LIG4 in each clinical sample with or without *FLT3*-ITD and *NPM1* mutation. Patient characteristics was shown in Table S2. The expression of DNA-PKcs and Ku80 were significantly increased in AML with *FLT3*-ITD, and the expression of DNA-PKcs and Ku70 were significantly increased in AML with *NPM1* mutation (Fig. S11A, B). Furthermore, when the expression of DNA-PKcs was compared among the 4 groups based on the presence or absence of *FLT3*-ITD and *NPM1* mutation, the expression was found to be significantly increased in cases positive for both *FLT3*-ITD and *NPM1* mutation, with a statistically significant difference (Fig. S11C). These findings suggest that AML with increased expression of NHEJ-related factors may have more chance to survive DNA damages that could result in mis-repair events leading to the generation of *FLT3*-ITD.

Expected model of *FLT3*-ITD generation

FLT3-ITD was previously thought to be created by genome slippage which hanged by microhomology (Fig. 5). However, this model did not fit the observation of clinical *FLT3*-ITDs because only a small portion of ITD clones had microhomology at the connection site of the ITD. In this study, we showed that the NHEJ process is indispensable for the creation of ITDs. We propose a model of *FLT3*-ITD generation based on these results (Fig. 5). The start and end of the ITD sequence did not fit at the exact sites of cleavage, and the ITD region accumulated in the middle of double nicks. A palindrome-like sequence confers a constitutively fragile structure, which frequently has nicks. Most of the SSBs would be completely repaired without any scar of the damage. However, contralateral double nicks could be separated as DSB with protruding ends. At the protruding cleavage site, elongation of the leading strand occurs simultaneously with DNA-end resection at the protruded end. If the replication speed overcomes the speed of DNA-end resection, replication forks passed each other and NHEJ creates ITDs. *FLT3*-ITD clones may be sometimes formed with a filler at the ITD junction in this process. On the other hand, if the DNA-end resection speed overcomes the speed of DNA replication, NHEJ creates deletions of various lengths. In both cases, NHEJ was initiated when the strands repaired to near blunt ends and joint the gap at the final step.

Discussion

FLT3 exon 14 has a cluster region of *FLT3*-ITD where the sequence exhibits a short inverted repeat sequence, a so-called palindrome-like sequence [19, 20, 29]. The distribution of the lengths of *FLT3*-ITD is between 3 bp and 400 bp, and the length always shows a multiple of 3, in-frame elongation [9, 10, 30]. *FLT3*-ITD can be oligoclonal and multiple *FLT3*-ITD clones and different clone sizes can exist in one case [4, 31]. Some cases acquired *FLT3*-ITD at relapse despite *FLT3*-ITD being absent at diagnosis [9-11]. These findings suggested that *FLT3*-ITD is later event after the leukemia initiating event. Furthermore, it has been suggested that patients with multiple *FLT3*-ITD clones have a poorer prognosis than that

for patients with a single *FLT3*-ITD clone [6, 32-34]. The poor prognostic impact of AML with *FLT3*-ITD might arise from the background genome instability, which yield *FLT3*-ITDs.

We deep sequenced clinical samples and revealed that the ITD start and end sites were clustered in a relatively short region flanking the palindrome-like sequence located on exon 14 of *FLT3*. Palindrome-like sequence sites can form a cruciform structure and are known to be genetically unstable and prone to acquire mutations [19]. We hypothesized that *FLT3*-ITDs are mis-repair events of genomic damage due to structural vulnerability. To elucidate the mechanism of *FLT3*-ITD generation, we examined the efficiency of *FLT3*-ITD generation by different modes of genome damage using the CRISPR/Cas9 system.

Contralateral double SSBs with distance of 50-100 bp efficiently repaired as tandem duplication in plants [35]. Based on the finding, we designed contralateral gRNAs with 53bp distance (Fig. 2C). We revealed that contralateral double nicks near the palindrome-like sequence repaired as *FLT3*-ITDs more efficiently than single SSB or DSB. The distributions of lengths of artificial *FLT3*-ITD clones were comparable among 3N, 3N+1, and 3N+2 bp. This suggests that ITDs other than in-frame mutations would be randomly generated and in-frame "3N" ITDs were eventually dominated in clinical samples, because only the in-frame 3N insertions confer a growth advantage. However, in our artificial *FLT3*-ITD model, we confirmed that none of the three cell lines expressed either *FLT3* transcript or protein. Therefore, our results represented immediate consequences of genome repair events without biological selection resulting from acquisition of *FLT3*-ITD. The joints of ITDs were categorized into 3 forms (Fig. S2). ITD without filler is the most frequent in clinical ITDs and in our experimental model. It was previously reported that a filler at the ITD joint was detected in 114 cases (38%) of 300 *FLT3*-ITD-positive AML cases [36]. Our model also showed *FLT3*-ITD with a filler in about around 11.2% to 19.8% in three cell lines.

It was reported that DSB with contralateral double nicks generated tandem duplication (TD) in the hypoxanthine phosphoribosyl transferase 1 (*HPRT*) gene in mouse embryonic stem cells [37], genic, intergenic and heterochromatic regions in Arabidopsis thaliana [35], and *FLT3* in human retinal pigment epithelial-1 (RPE-1) cells [38]. However, differences in the repair patterns have not been investigated by using a clinical-grade specific inhibitor targeting the DNA repair pathway. Olaparib and peposertib are clinically available inhibitors of PARP and DNA-PKcs, which inhibit the repair of SSBs and DSBs, respectively. Olaparib is a selective inhibitor of PARP1/2, which is clinically used for *BRCA1/2* mutated tumors such as ovarian, breast, and prostate cancers. *BRCA1/2* is indispensable for the error-free homologous recombination (HR) process. PARP1/2 are involved in the SSB repair process, and inhibition of PARP1/2 therefore cause persistence of the SSB, which is eventually converted to a DSB during the DNA replication process and causes synthetic lethality in tumors with HR deficiency such as *BRCA1/2* mutated tumors [22]. However, olaparib had no effect on either mutation frequency or *FLT3*-ITD generation. Peposertib selectively inhibits autophosphorylation of DNA-PKcs, which is one of the key drivers in NHEJ [23, 24]. Peposertib leads to persistence of unrepaired DSBs and enhances the antitumor activity of DSB-inducing agents such as ionizing radiation (IR) and topoisomerase II inhibitors in some cancers [39-41]. Peposertib is currently in clinical trials for advanced solid tumors (NCT02516813) and in combination with chemotherapy for relapse and refractory AML (NCT03983824). We showed that the mutation frequency and the rate of repair as *FLT3*-ITD

were significantly reduced by administration of peposertib in HEK293T cells and K562 cells. These results suggested that NHEJ is essential for *FLT3*-ITD generation.

The generation of TD has been explained by replication slippage [35, 36, 42]. The classical slippage model can explain ITD with microhomology, however, the majority of clinical and experimental ITDs did not have microhomology. Furthermore, slippage model should be suppressed by olaparib because the process needs base excision repair at the final process (Fig. 5). Our observation did not support slippage model. On the other hand, full-length ITDs spanning the cleavage site were scarce in our experimental model. Based on our experimental observations, we presented a novel model in which nibbling of the free single strand and replication occurred simultaneously following NHEJ of the blunt ends. Depending on the speed of nibbling and replication, the repair can resulted in ITD or deletion. Contralateral double nicks creates DSB with protruding ends and staggered strand is repaired or trimmed following jointed by NHEJ.

Certain genetic backgrounds such as *NPM1* mutation, *NUP98::NSD1*, *DEK::NUP214, UBTF*-ITD were commonly accompanied *FLT3*-ITD in AML [25-27, 43]. In our study, we found increased expression of DNA-PKcs in ITD-positive and *NPM1* mutation-positive cases. It is known that acquisition of *FLT3*-ITD increases reactive oxygen species (ROS) production and DSBs, and increases DNA-PK activity [44]. It has also been reported that DNA-PK activity correlates with DNA-PKcs expression [45, 46]. Our study showed that the expression of DNA-PKcs was significantly increased in AML with *FLT3*-ITD and/or *NPM1* mutation. *FLT3*-ITD may be more likely to be generated when DNA damages were repaired by NHEJ. Treatment with peposertib combined with cytotoxic chemotherapy might not only enhance the cytotoxic effect of chemotherapy but also suppress the development of de-novo *FLT3*-ITD formation.

In conclusion, repair of contralateral double nicks at *FLT3* exon 14 flanking the palindrome-like sequence generates *FLT3*-ITD via NHEJ. This is the first study clarifying the detailed mechanisms of the generation of *FLT3*-ITD mutation by using a clinical-grade specific inhibitor targeting the DNA repair pathway. Our model highlighted the importance of the NHEJ process, which was not focused on in the previous slippage model.

Acknowledgments

We thank Fumina Kusaka and Chiaki Yokoyama for management of patients' samples and maintenance of data integrity.

Authorship Contributions

S. Yoshida., M.O. and S. Yokoyama design the experiment. S. Yoshida, and M.O. analyzed data and wrote the draft manuscript; All authors provided intellectual input and revised and gave final approval to the manuscript.

Disclosure of Conflicts of Interest

The authors declare no conflict of interest.

FUNDING

This work was supported by the Japan Society for the Promotion of Science (JSPS), “Grant-in-Aid for scientific research (C) (M.O; 20K08745) and research grant of Nippon Kayaku (M.O; NKCS20240403002).

Data Availability Statement

The datasets for this study are available from the corresponding author on reasonable request.

References

[1] Grimwade D, Ivey A, Huntly BJ. Molecular landscape of acute myeloid leukemia in younger adults and its clinical relevance. Blood. 2016;127:29-41.

[2] Papaemmanuil E, Gerstung M, Bullinger L, et al. Genomic Classification and Prognosis in Acute Myeloid Leukemia. N Engl J Med. 2016;374:2209-2221.

[3] Grundler R, Miething C, Thiede C, Peschel C, Duyster J. FLT3-ITD and tyrosine kinase domain mutants induce 2 distinct phenotypes in a murine bone marrow transplantation model. Blood. 2005;105:4792-4799.

[4] Rebechi MT, Pratz KW. Genomic instability is a principle pathologic feature of FLT3 ITD kinase activity in acute myeloid leukemia leading to clonal evolution and disease progression. Leuk Lymphoma. 2017;58:1-11.

[5] Kiyoi H, Naoe T, Nakano Y, et al. Prognostic implication of FLT3 and N-RAS gene mutations in acute myeloid leukemia. Blood. 1999;93:3074-3080.

[6] Kottaridis PD, Gale RE, Frew ME, et al. The presence of a FLT3 internal tandem duplication in patients with acute myeloid leukemia (AML) adds important prognostic information to cytogenetic risk group and response to the first cycle of chemotherapy: analysis of 854 patients from the United Kingdom Medical Research Council AML 10 and 12 trials. Blood. 2001;98:1752-1759.

[7] Daver N, Schlenk RF, Russell NH, Levis MJ. Targeting FLT3 mutations in AML: review of current knowledge and evidence. Leukemia. 2019;33:299-312.

[8] Kottaridis PD, Gale RE, Langabeer SE, Frew ME, Bowen DT, Linch DC. Studies of FLT3 mutations in paired presentation and relapse samples from patients with acute myeloid leukemia: implications for the role of FLT3 mutations in leukemogenesis, minimal residual disease detection, and possible therapy with FLT3 inhibitors. Blood. 2002;100:2393-2398.

[9] Shih LY, Huang CF, Wu JH, et al. Internal tandem duplication of FLT3 in relapsed acute myeloid leukemia: a comparative analysis of bone marrow samples from 108 adult patients at diagnosis and relapse. Blood. 2002;100:2387-2392.

[10] Wakita S, Yamaguchi H, Omori I, et al. Mutations of the epigenetics-modifying gene (DNMT3a, TET2, IDH1/2) at diagnosis may induce FLT3-ITD at relapse in de novo acute myeloid leukemia. Leukemia. 2013;27:1044-1052.

[11] McCormick SR, McCormick MJ, Grutkoski PS, et al. FLT3 mutations at diagnosis and relapse in acute myeloid leukemia: cytogenetic and pathologic correlations, including cuplike blast morphology. Arch Pathol Lab Med. 2010;134:1143-1151.

[12] Perl AE, Martinelli G, Cortes JE, et al. Gilteritinib or Chemotherapy for Relapsed or Refractory FLT3-Mutated AML. N Engl J Med. 2019;381:1728-1740.

[13] Cortes JE, Khaled S, Martinelli G, et al. Quizartinib versus salvage chemotherapy in relapsed or refractory FLT3-ITD acute myeloid leukaemia (QuANTUM-R): a multicentre, randomised, controlled, open-label, phase 3 trial. Lancet Oncol. 2019;20:984-997.

[14] Erba HP, Montesinos P, Kim HJ, et al. Quizartinib plus chemotherapy in newly diagnosed patients with FLT3-internal-tandem-duplication-positive acute myeloid leukaemia (QuANTUM-First): a randomised, double-blind, placebo-controlled, phase 3 trial. Lancet. 2023;401:1571-1583.

[15] Sallmyr A, Fan J, Datta K, et al. Internal tandem duplication of FLT3 (FLT3/ITD) induces increased ROS production, DNA damage, and misrepair: implications for poor prognosis in AML. Blood. 2008;111:3173-3182.

[16] Pikor L, Thu K, Vucic E, Lam W. The detection and implication of genome instability in cancer. Cancer Metastasis Rev. 2013;32:341-352.
[17] Yoshida S, Onozawa M, Miyashita N, et al. Clinical features of complex karyotype in newly diagnosed acute myeloid leukemia. Int J Hematol. 2023;117:544-552.
[18] Kanda Y. Investigation of the freely available easy-to-use software 'EZR' for medical statistics. Bone Marrow Transplant. 2013;48:452-458.
[19] Lu S, Wang G, Bacolla A, Zhao J, Spitser S, Vasquez KM. Short Inverted Repeats Are Hotspots for Genetic Instability: Relevance to Cancer Genomes. Cell Rep. 2015;10:1674-1680.
[20] Finnon R, Brown N, Moody J, et al. Flt3-ITD mutations in a mouse model of radiation-induced acute myeloid leukaemia. Leukemia. 2012;26:1445-1446.
[21] Novak RL, Harper DP, Caudell D, Slape C, Beachy SH, Aplan PD. Gene expression profiling and candidate gene resequencing identifies pathways and mutations important for malignant transformation caused by leukemogenic fusion genes. Exp Hematol. 2012;40:1016-1027.
[22] Ali U, Vungarala S, Tiriveedhi V. Genomic Features of Homologous Recombination Deficiency in Breast Cancer: Impact on Testing and Immunotherapy. Genes (Basel). 2024;15.
[23] Matsumoto Y. Development and Evolution of DNA-Dependent Protein Kinase Inhibitors toward Cancer Therapy. Int J Mol Sci. 2022;23.
[24] Schimmel J, Munoz-Subirana N, Kool H, et al. Modulating mutational outcomes and improving precise gene editing at CRISPR-Cas9-induced breaks by chemical inhibition of end-joining pathways. Cell Rep. 2023;42:112019.
[25] Sandahl JD, Coenen EA, Forestier E, et al. t(6;9)(p22;q34)/DEK-NUP214-rearranged pediatric myeloid leukemia: an international study of 62 patients. Haematologica. 2014;99:865-872.
[26] Hollink IH, van den Heuvel-Eibrink MM, Arentsen-Peters ST, et al. NUP98/NSD1 characterizes a novel poor prognostic group in acute myeloid leukemia with a distinct HOX gene expression pattern. Blood. 2011;118:3645-3656.
[27] Kronke J, Bullinger L, Teleanu V, et al. Clonal evolution in relapsed NPM1-mutated acute myeloid leukemia. Blood. 2013;122:100-108.
[28] Bezerra MF, Lima AS, Pique-Borras MR, et al. Co-occurrence of DNMT3A, NPM1, FLT3 mutations identifies a subset of acute myeloid leukemia with adverse prognosis. Blood. 2020;135:870-875.
[29] Kiyoi H, Towatari M, Yokota S, et al. Internal tandem duplication of the FLT3 gene is a novel modality of elongation mutation which causes constitutive activation of the product. Leukemia. 1998;12:1333-1337.
[30] Breitenbuecher F, Schnittger S, Grundler R, et al. Identification of a novel type of ITD mutations located in nonjuxtamembrane domains of the FLT3 tyrosine kinase receptor. Blood. 2009;113:4074-4077.
[31] Yokoyama S, Onozawa M, Yoshida S, et al. Subclinical minute FLT3-ITD clone can be detected in clinically FLT3-ITD-negative acute myeloid leukaemia at diagnosis. Br J Haematol. 2023.
[32] Schranz K, Hubmann M, Harin E, et al. Clonal heterogeneity of FLT3-ITD detected by high-throughput amplicon sequencing correlates with adverse prognosis in acute myeloid leukemia. Oncotarget. 2018;9:30128-30145.
[33] Gale RE, Green C, Allen C, et al. The impact of FLT3 internal tandem duplication mutant level, number, size, and interaction with NPM1 mutations in a large cohort of young adult patients with acute myeloid leukemia. Blood. 2008;111:2776-2784.

[34] Borthakur G, Kantarjian H, Patel KP, et al. Impact of numerical variation in FMS-like tyrosine kinase receptor 3 internal tandem duplications on clinical outcome in normal karyotype acute myelogenous leukemia. Cancer. 2012;118:5819-5822.
[35] Schiml S, Fauser F, Puchta H. Repair of adjacent single-strand breaks is often accompanied by the formation of tandem sequence duplications in plant genomes. Proc Natl Acad Sci U S A. 2016;113:7266-7271.
[36] Borrow J, Dyer SA, Akiki S, Griffiths MJ. Terminal deoxynucleotidyl transferase promotes acute myeloid leukemia by priming FLT3-ITD replication slippage. Blood. 2019;134:2281-2290.
[37] Schimmel J, Kool H, van Schendel R, Tijsterman M. Mutational signatures of non-homologous and polymerase theta-mediated end-joining in embryonic stem cells. EMBO J. 2017;36:3634-3649.
[38] Schimmel J, Munoz-Subirana N, Kool H, van Schendel R, Tijsterman M. Small tandem DNA duplications result from CST-guided Pol alpha-primase action at DNA break termini. Nat Commun. 2021;12:4843.
[39] Haines E, Nishida Y, Carr MI, et al. DNA-PK inhibitor peposertib enhances p53-dependent cytotoxicity of DNA double-strand break inducing therapy in acute leukemia. Sci Rep. 2021;11:12148.
[40] Gordhandas SB, Manning-Geist B, Henson C, et al. Pre-clinical activity of the oral DNA-PK inhibitor, peposertib (M3814), combined with radiation in xenograft models of cervical cancer. Sci Rep. 2022;12:974.
[41] Patterson-Fortin J, Bose A, Tsai WC, et al. Targeting DNA Repair with Combined Inhibition of NHEJ and MMEJ Induces Synthetic Lethality in TP53-Mutant Cancers. Cancer Res. 2022;82:3815-3829.
[42] Vaughn JN, Bennetzen JL. Natural insertions in rice commonly form tandem duplications indicative of patch-mediated double-strand break induction and repair. Proc Natl Acad Sci U S A. 2014;111:6684-6689.
[43] Kaburagi T, Shiba N, Yamato G, et al. UBTF-internal tandem duplication as a novel poor prognostic factor in pediatric acute myeloid leukemia. Genes Chromosomes Cancer. 2023;62:202-209.
[44] Murray HC, Enjeti AK, Kahl RGS, et al. Quantitative phosphoproteomics uncovers synergy between DNA-PK and FLT3 inhibitors in acute myeloid leukaemia. Leukemia. 2021;35:1782-1787.
[45] Someya M, Sakata K, Matsumoto Y, et al. The association of DNA-dependent protein kinase activity with chromosomal instability and risk of cancer. Carcinogenesis. 2006;27:117-122.
[46] Ihara M, Ashizawa K, Shichijo K, Kudo T. Expression of the DNA-dependent protein kinase catalytic subunit is associated with the radiosensitivity of human thyroid cancer cell lines. J Radiat Res. 2019;60:171-177.

Figure Legends

Figure 1. Deep sequence of the clinical *FLT3*-ITD cluster region

A. Start and end positions of *FLT3*-ITD identified in 20 clinical samples are shown. The blue line and the red line show the start and end positions of *FLT3*-ITD in each clone. "＊" represents the palindrome-like sequence.
B. A 30 base-pair incomplete palindrome sequence was identified in the middle of the *FLT3*-ITD cluster region of *FLT3* exon 14.

C. Accumulations of areas of *FLT3*-ITD and deletions found in clinical samples are shown. "＊" represents the palindrome-like sequence.
D. Distribution of variant allele frequencies of *FLT3*-ITDs and deletions is shown. Statistical significance was calculated by the Mann-Whitney U test (*P<0.001)
E. Distribution of the lengths of *FLT3*-ITDs.
F. Percentages of length categories of clinical *FLT3*-ITDs. The lengths of most of the *FLT3*-ITDs were multiply of 3 (3N).
G. Joint characteristics of *FLT3*-ITDs found in clinical samples.

Figure 2. Artificial *FLT3*-ITD generation by the CRISPR/Cas9 system

A. Doxycycline-inducible CRISPR/Cas9 transposon vector and piggyBac transposase vector were co-transfected into cells. After puromycin-selection, bulk cells were used for an artificial *FLT3*-ITD generation study. Doxycycline was administered to induce the expression of Cas9 followed by gRNA transfection 24 hr later.
CEH, CMV enhancer; IRES, internal ribosome entry site; ITR, inverted terminal repeat sequences; PAC, puromycin N-acetyltransferase; rtTA3, reverse tetracycline transactivator; TRE, tetracycline-responsive elements
B. Four modes of DNA damage were induced by the combination of Cas9 and gRNA. Single DSB, double DSBs, single SSB, and double SSBs (contralateral double nicks) were compared. The blue bar indicates Proto-spacer Adjacent Motif (PAM). DSB, double-strand break; SSB, single-strand break
C. Two gRNAs were designed to target contralateral flanking sites of the palindrome-like sequence at human *FLT3* exon 14.
AS, Antisense strand; S, Sense strand
D. Examples of artificial *FLT3*-ITD sequences obtained in K562 cell line are shown. The underlined parts are the ITD sites. The sequence highlighted in blue, yellow and green indicate Proto-spacer Adjacent Motif (PAM), filler and microhomology, respectively.

Figure 3. Comparison of the efficiencies of artificial *FLT3*-ITD generation by different modes of DNA damage in HEK293T cells and K562 cells

A. Comparison of mutation frequencies and mutation rates by different modes of DNA breaks. Because the mutation frequency of single SSB was very low, the mutation rate is not shown. Independent experiments were performed three times. Data for mutation frequency are shown as means ± SD.

B. Area of *FLT3*-ITDs with VAF of more than 0.01% is shown. Orange lines show positions of gRNAs. "＊" represents the palindrome-like sequence.

C. Distribution of ITD lengths for each cell line. HEK293T: median length of 18 bp (3-84 bp); K562: median length of 22 bp (3-75 bp).

D. Percentages of length categories of artificial *FLT3*-ITDs. *FLT3*-ITD lengths were equally distributed among 3N, 3N+1, and 3N+2 bp.

E. Percentages of joint characteristics of artificial *FLT3*-ITDs.

Figure 4. Comparison of the efficiencies of *FLT3*-ITD generation by administration of olaparib or peposertib

A. Cas9-D10A was expressed with double gRNAs with or without olaparib (20 μM). Olaparib was administered 48 hours prior to transfection of gRNAs. Cells were harvested at 48 hr after transfection of gRNAs. Western blotting showed a higher level of γ-H2AX expression in olaparib-treated cells (upper). The mutation frequency and mutation rate are shown (bottom). Independent experiments were performed three times. Data of mutation frequency are shown as means ± SD.
B. Cas9-D10A was expressed with double gRNAs with or without peposertib (2 μM). Peposertib was administered 45 min prior to transfection of gRNAs. Cells were harvested at 4, 8, 12 hours after transfection of gRNAs for Western blotting and at 48 hr after transfection of gRNAs for mutation analysis. Western blotting showed successful suppression of phosphorylated DNA PKcs (upper). The mutation frequency and mutation rate are shown (bottom). Independent experiments were performed three times. Data of mutation frequency are shown as means ± SD.
C. Double gRNAs were transfected into K562 cells expressing Cas9-D10A, with or without DNA-PKcs knockout. Western blotting showed knocking out of DNA-PKcs (left). The mutation frequency and mutation rate are shown (right). Independent experiments were performed three times. Data of mutation frequency are shown as means ± SD.

Figure 5. Expected model of *FLT3*-ITD generation

Proposal model of *FLT3*-ITD generation is shown. Contralateral double nicks resulted in DSB with protruding ends. If nicks repaired by base excision repair (BER) before it become DSB, or DSB with protruding ends repaired by homologous recombination, the breaks were repaired completely without any scar. Without immediate SSB repair, contralateral double nicks resulted in DSB with 2 protruding ends. Elongation in the leading strand occurs simultaneously with DNA-end resection of the protruding strand. When both ends repaired up to near blunt DSB, non-homologous end joining (NHEJ) process is initiated. ITD or deletion is formed depending on the dominancy of polymerase or nuclease functions. If polymerase is dominant compared to DNA-end resection, replication forks pass each other to create ITD. NHEJ is indispensable for joining the blunt ends with or without a filler in the final step. This model explains why the duplicated region did not exactly match to cleavage sites and was always located within cleavage sites. The orange line indicates where ITD is expected to form. Previous genome slippage model needs BER at the final process, however BER inhibitor, Olaparib, did not suppress generation of ITDs. *FLT3*-ITD with microhomology consisted only small fraction of both clinical and experimental ITDs (Fig 1G, 3E).

564 BER, base excision repair; DSB, double-strand break; HR, homologous recombination; NHEJ,
565 non-homologous end joining; SSB, single-strand break

Figure 1

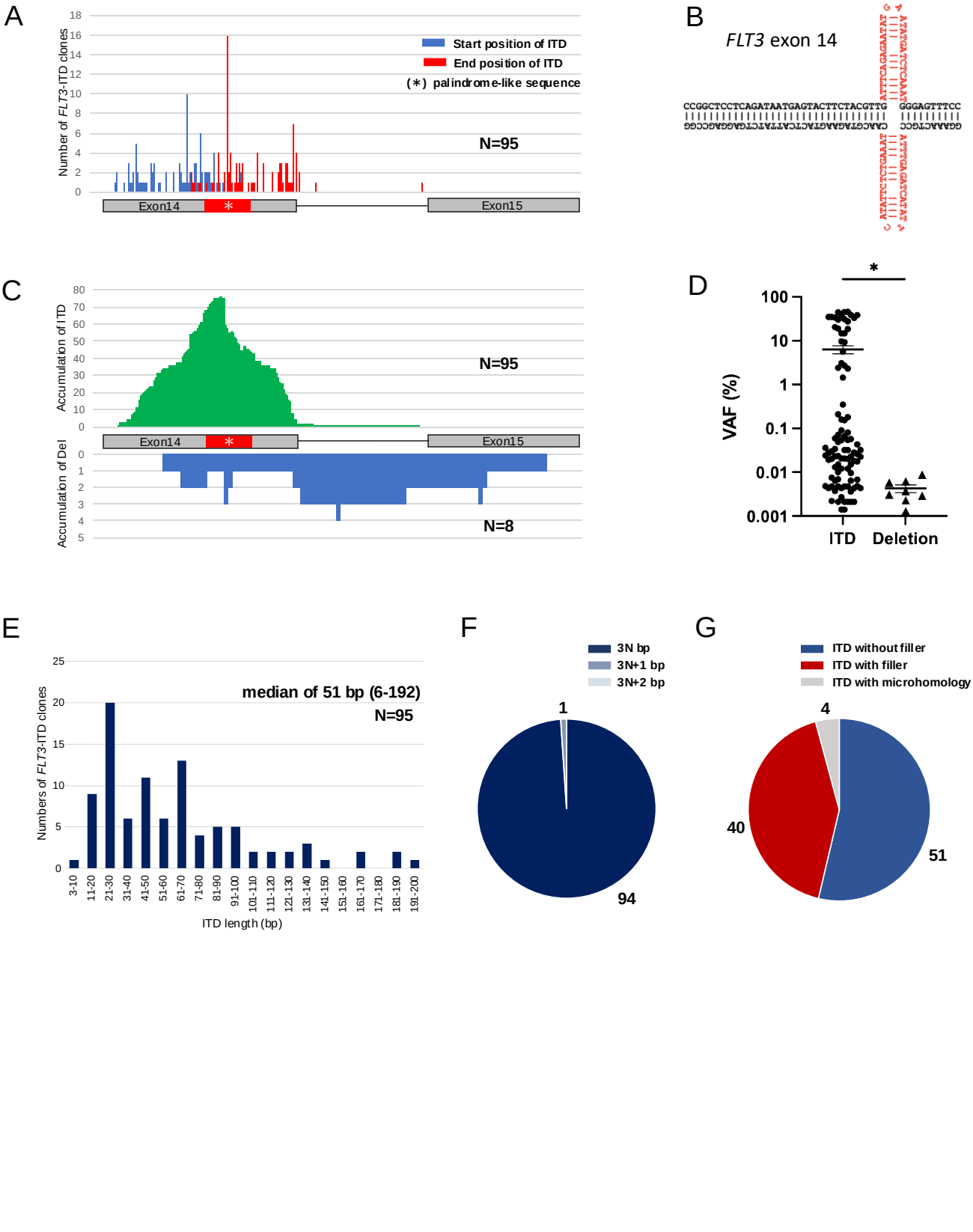

Figure 2

A

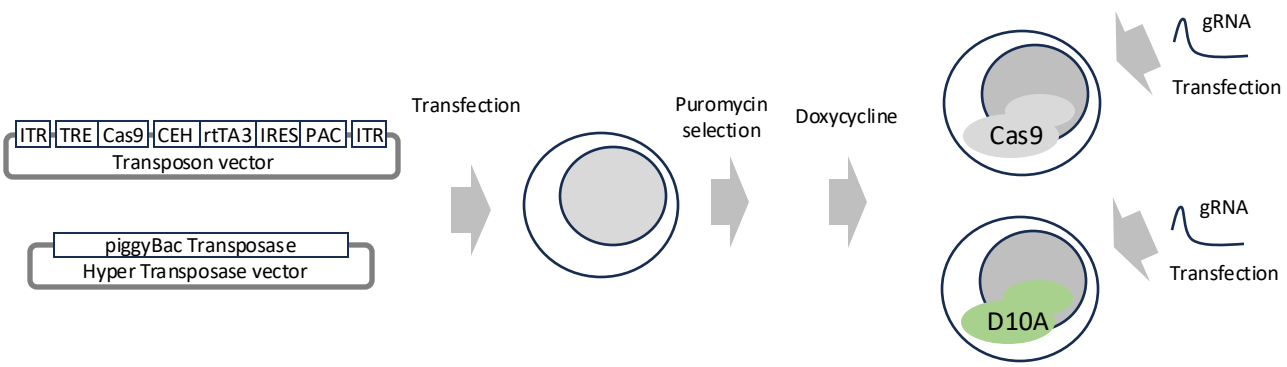

B

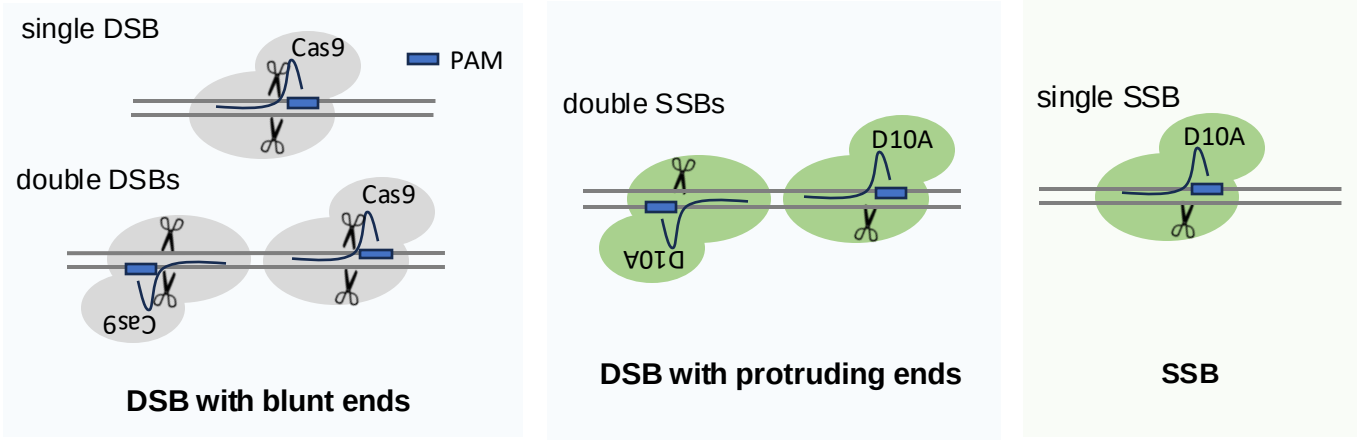

C

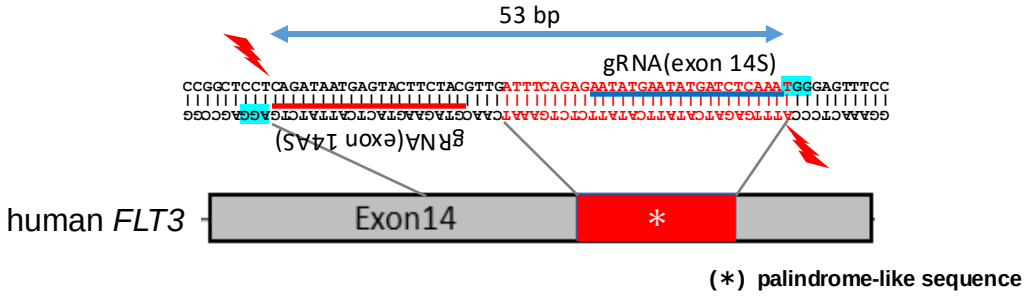

(*) palindrome-like sequence

D

CCGGCTCCTCAGATAATGAGTACTTCTACGTTGATTATAATGAGTACTTCTACGTTGATTTCAGAGAATATGAATATGATCTCAAATGGGAGTTTCC (24bp)

CCGGCTCCTCAGATAATGAGTACTTCTACGTTGATTTCAGAGAATATGAATATGATCTCGTTGATTTCAGAGAATATGAATATGATCTCAAATGGGAGTTTCC (30bp)

CCGGCTCCTCAGATAATGAGTACTTCTACGTTGATTTCAGAGAATATGAATATGATCTCGAGTACTTCTACGTTGATTTCAGAGAATATGAATATGATCTCAAATGGGAGTTTCC (42bp)

CCGGCTCCTCAGATAATGAGTACTTCTACGTTGATTTCATAATGAGTACTTCTACGTTGATTTCAGAGAATATGAATATGATCTCAAATGGGAGTTTCC (26bp)

CCGGCTCCTCAGATAATGAGTACTTCTACGTTGATTTCAGAGAATATGAATATGATCTCTGAGTACTTCTACGTTGATTTCAGAGAATATGAATATGATCTCAAATGGGAGTTTCC (43bp)

CCGGCTCCTCAGATAATGAGTACTTCTACGTTGATTTCAGAGAATATGAATATGATCTCATAATGAGTACTTCTACGTTGATTTCAGAGAATATGAATATGATCTCAAATGGGAGTTTCC (47bp)

CCGGCTCCTCAGATAATGAGTACTTCTACGTTGATTTCAGAGAATATGAATACTCAGTTGATTTCAGAGAATATGAATATGATCTCAAATGGGAGTTTCC (27bp)

CCGGCTCCTCAGATAATGAGTACTTCTACGTTGATTTCAGAGATCATATAATGAGTACTTCTACGTTGATTTCAGAGAATATGAATATGATCTCAAATGGGAGTTTCC (35bp)

CCGGCTCCTCAGATAATGAGTACTTCTACGTTGATTTCAGAGAATACTTCTACGTTGATTTCAGAGAATATGAATATGATCTCAAATGGGAGTTTCC (24bp)

CCGGCTCCTCAGATAATGAGTACTTGTACGTTGATTTCAGAGAATATGAATATGATGTACGTTGATTTCAGAGAATATGAATATGATCTCAAATGGGAGTTTCC (31bp)

PAM Filler microhomology

Figure 3

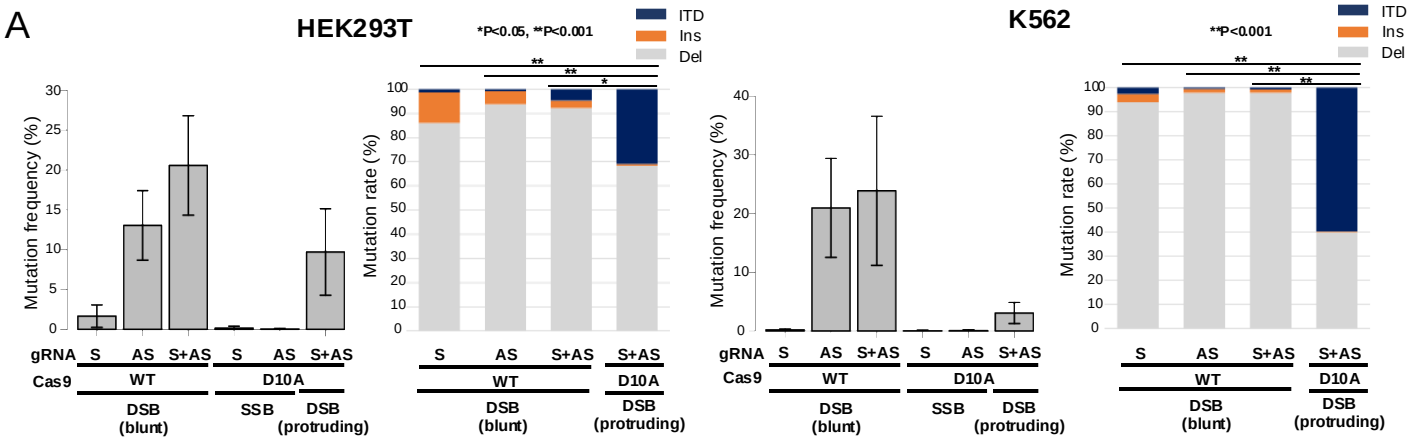
A
HEK293T
*P<0.05, **P<0.001
ITD
Ins
Del
Mutation frequency (%)
Mutation rate (%)
gRNA S AS S+AS S AS S+AS
Cas9 WT D10A
DSB (blunt)
SSB
DSB (protruding)
K562
**P<0.001

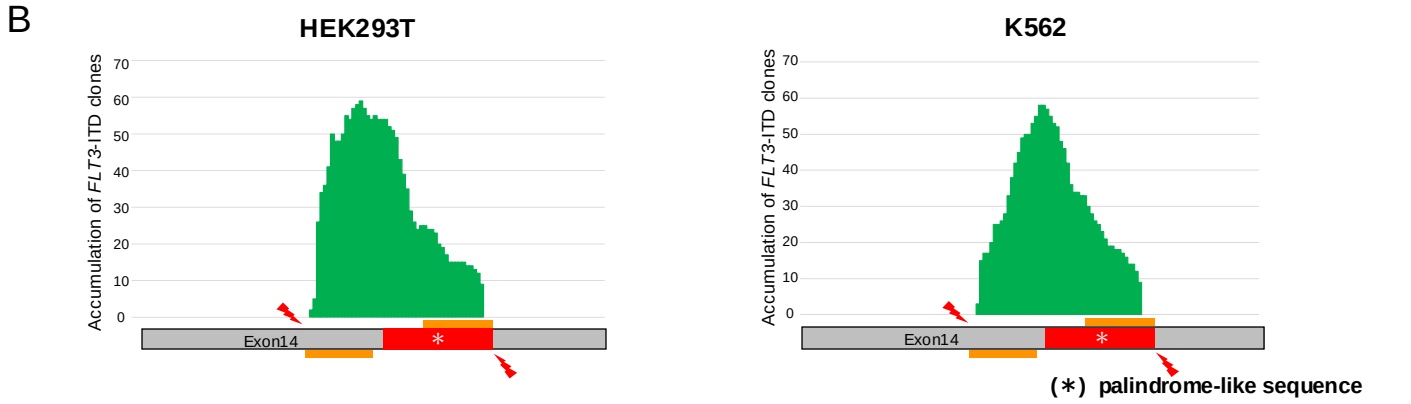
B
HEK293T
K562
Accumulation of FLT3-ITD clones
Exon14
(*) palindrome-like sequence

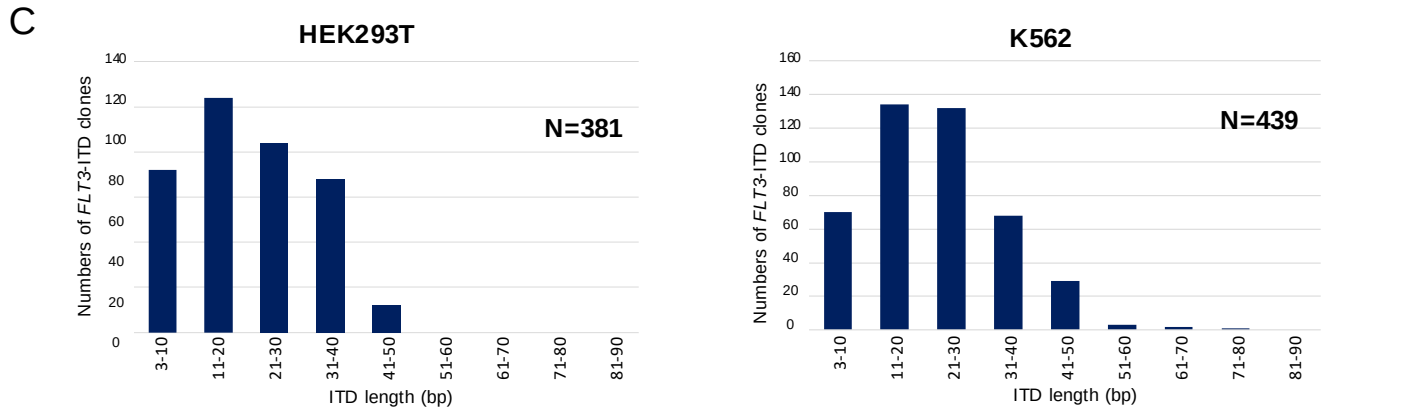
C
HEK293T
N=381
K562
N=439
Numbers of FLT3-ITD clones
ITD length (bp)
3-10
11-20
21-30
31-40
41-50
51-60
61-70
71-80
81-90

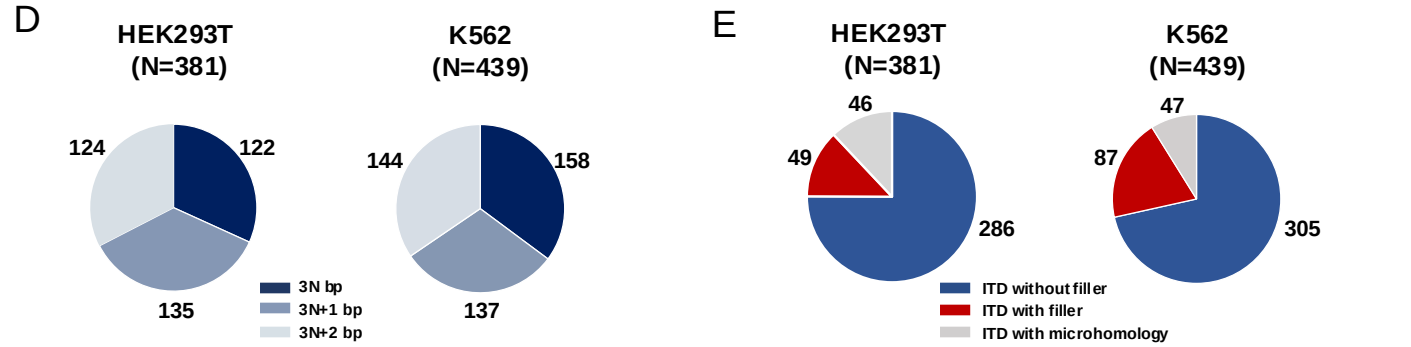
D
HEK293T (N=381)
K562 (N=439)
124
122
135
144
158
137
3N bp
3N+1 bp
3N+2 bp
E
HEK293T (N=381)
K562 (N=439)
46
49
286
47
87
305
ITD without filler
ITD with filler
ITD with microhomology

Figure 4

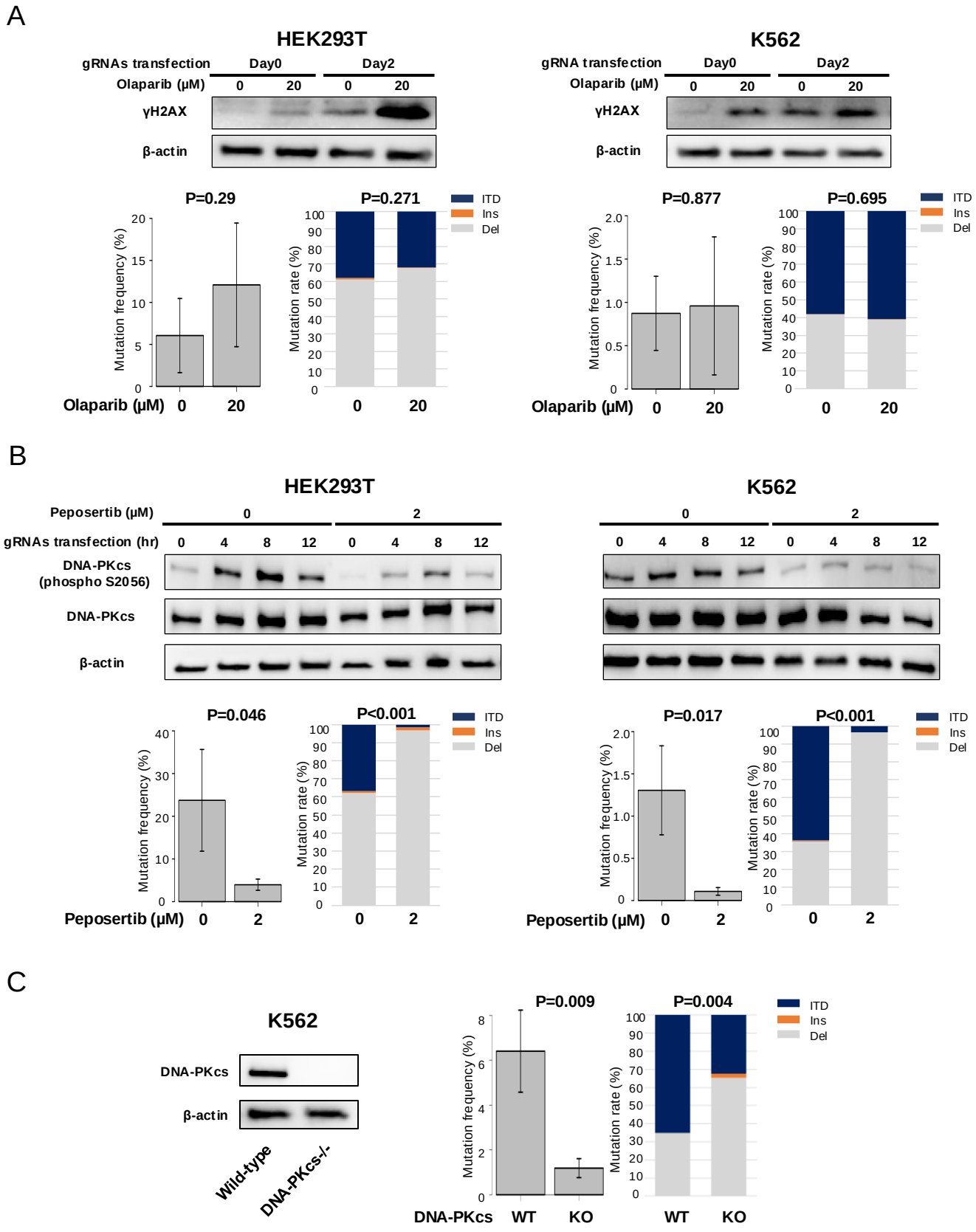
A
HEK293T
gRNAs transfection
Day0
Day2
Olaparib (μM)
0
20
0
20
γH2AX
β-actin
P=0.29
P=0.271
ITD
Ins
Del
Mutation frequency (%)
Mutation rate (%)
Olaparib (μM)
0
20
K562
gRNA transfection
P=0.877
P=0.695
B
HEK293T
Peposertib (μM)
gRNAs transfection (hr)
0
4
8
12
DNA-PKcs (phospho S2056)
DNA-PKcs
β-actin
P=0.046
P<0.001
Peposertib (μM)
K562
P=0.017
C
K562
DNA-PKcs
β-actin
Wild-type
DNA-PKcs-/-
P=0.009
P=0.004
DNA-PKcs
WT
KO

Figure 5

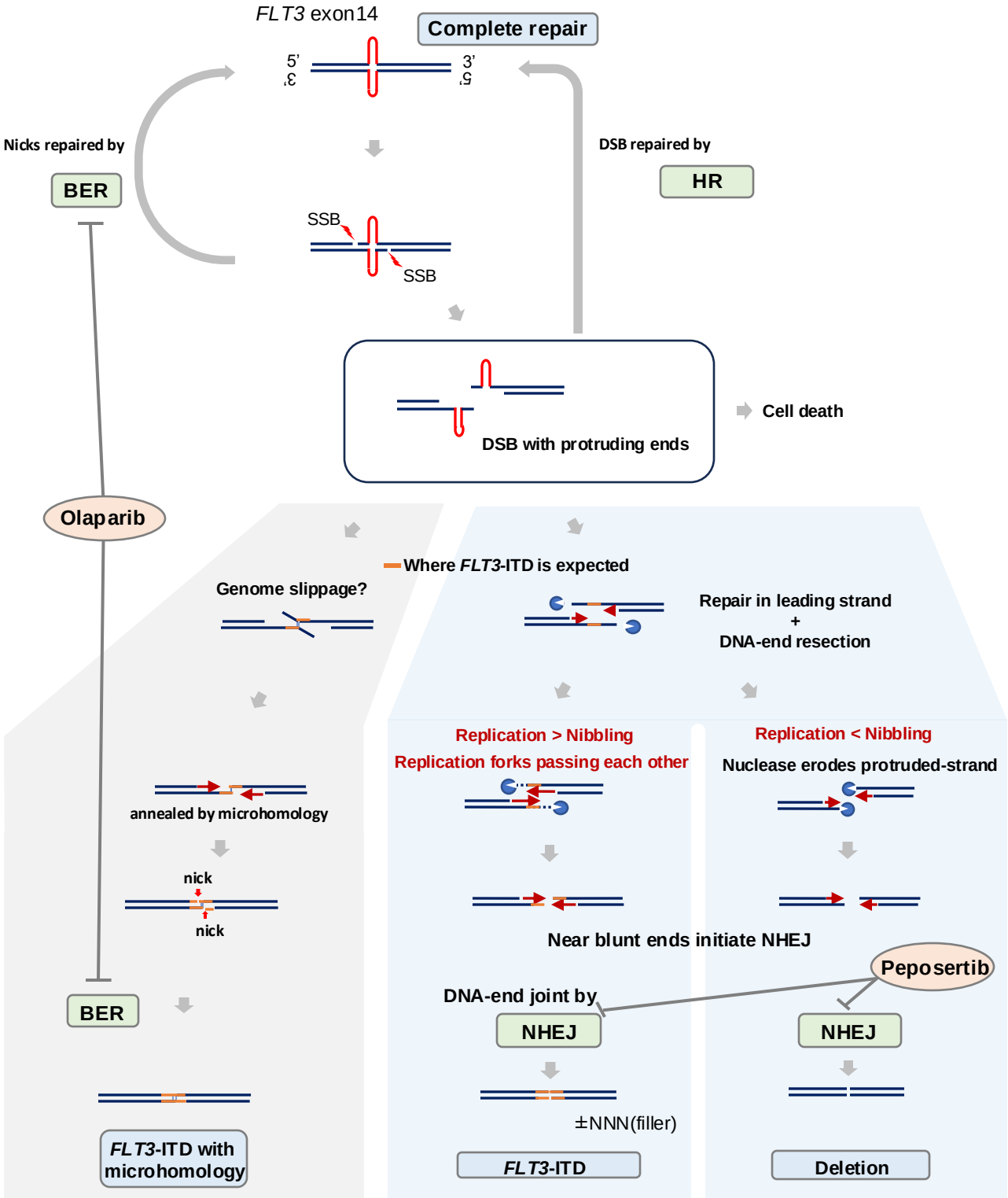
FLT3 exon14
Complete repair
5'
3'
Nicks repaired by
BER
DSB repaired by
HR
SSB
SSB
DSB with protruding ends
Cell death
Olaparib
Where FLT3-ITD is expected
Genome slippage?
Repair in leading strand
+
DNA-end resection
Replication > Nibbling
Replication forks passing each other
Replication < Nibbling
Nuclease erodes protruded-strand
annealed by microhomology
nick
nick
Near blunt ends initiate NHEJ
Peposertib
DNA-end joint by
NHEJ
NHEJ
BER
±NNN(filler)
FLT3-ITD with microhomology
FLT3-ITD
Deletion